

Controlled Synthesis of Near-Stoichiometric Cobalt Ferrite Nanoparticles

Richard T. Olsson,[†] German Salazar-Alvarez,[‡] Mikael S. Hedenqvist,[†] Ulf W. Gedde,^{*,†}
Fredrik Lindberg,[§] and Steven J. Savage^{||}

Fibre and Polymer Technology, and Materials Science and Engineering, Royal Institute of Technology,
SE-100 44 Stockholm, Sweden, Structural Chemistry, Arrhenius Laboratory, Stockholm University,
SE-106 91 Stockholm, Sweden, and Swedish Defense Research Agency (FOI), P.O. Box 1165,
SE-581 11 Linköping, Sweden

Received January 24, 2005. Revised Manuscript Received May 4, 2005

Large batches of more than 18 g of cobalt ferrite nanoparticles ($\text{Co}_x\text{Fe}_{3-x}\text{O}_4$, x being close to 1) have been prepared by the “chemie douce approach” using aqueous solutions of metal salts at 90 °C mixed with solutions of hydroxide ions under air atmosphere. By suitable choice of the metal ion to hydroxide ion ratio, it was possible to prepare nanoparticles with the stoichiometric composition (CoFe_2O_4). The composition and the density of the nanoparticles could be controlled by varying the metal ion to hydroxide ion molar ratio in the reactor. Adjusting the initial concentration ratios of the reactants prior to the mixing allowed the variation of the average size of the nanoparticles. The repeatability of the average particle diameter of the synthesis was typically 5 nm and average particle sizes could be controlled between 50 and 80 nm determined by nitrogen adsorption measurements (consistent with the number size average 35–60 nm obtained by transmission electron microscopy studies). Aging of the suspensions resulted in a narrowing of the initial broad unimodal distribution. The narrowing of the size distribution was associated with the phase transformation of δ -FeOOH platelets to spinel phase. The spinel nanoparticles had different morphologies: cubic, spherical, and occasionally irregular. Nanoparticles with the stoichiometric composition were a mixture of cubical and spherical shapes. Nanoparticles with less than the stoichiometric cobalt content had an irregular morphology, whereas nanoparticles with greater than the stoichiometric concentration of cobalt were predominantly spherical.

1. Introduction

Spinel ferrites are important commercial electroceramics, and in the past 2 decades many applications have emerged using these materials in the form of nanoparticles.¹ Ferrites have received attention as a result of their magnetic^{2,3} and electronic properties.⁴ Ferrites are currently used in magnetic recording media,⁵ biomedicine,⁶ microwave devices,⁷ and contrast enhancers in magnetic resonance imaging.⁸ The current interest in nanoparticle ferrites arises from the particular advantages to be obtained from integrating the nanoparticle ferrites into polymer matrixes, to produce multifunctional nanocomposites.

Ferrite nanoparticles have been prepared by sonochemical reactions,⁹ by mechanochemical synthesis,^{10–12} by hydrolysis of precursors,^{13,14} by flow injection synthesis,¹⁵ and in the confined zones of microemulsions,¹⁶ in polymeric matrixes,^{17,18} and by aqueous coprecipitation.^{19,20} In most cases, cobalt ferrite nanoparticles have been prepared by coprecipitating a mixture of cobalt(II) and iron(II) ions with hydroxide ions using air²¹ or potassium nitrate¹⁹ as oxidizing agent similar to the preparation of magnetite nanoparticles (Fe_3O_4).²² Aqueous coprecipitation has proven to be an economic and versatile technique suitable to synthesis of

* Corresponding author. E-mail: gedde@polymer.kth.se.
[†] Fibre and Polymer Technology, Royal Institute of Technology.
[‡] Materials Science and Engineering, Royal Institute of Technology.
[§] Stockholm University.
^{||} Swedish Defense Research Agency (FOI).
 (1) Sugimoto, M. *J. Am. Ceram. Soc.* **1999**, *82*, 269.
 (2) Rondinone, A. J.; Samia, A. C. S.; Zhang, Z. *J. Appl. Phys. Lett.* **2000**, *76*, 3624.
 (3) Rondinone, A. J.; Samia, A. C. S.; Zhang, Z. *J. Phys. Chem. B* **1999**, *103*, 6876.
 (4) Smit, J.; Wijn, H. P. J. *Ferrites: physical properties of ferri-magnetic oxides in their relation to their technical applications*; Philips: Eindhoven, The Netherlands, 1959.
 (5) Simonds, J. L. *Phys. Today* **1995**, *48*, 26.
 (6) Häfeli, U.; Schütt W.; Teller J.; Zborowski M. *Scientific and clinical applications of magnetic carriers*; Kluwer Academic Press/Plenum Publishers: Amsterdam, 1997.
 (7) Pardavi-Horvath, M. *J. Magn. Magn. Mater.* **2000**, *215–216*, 171.
 (8) Hogemann, D.; Josephson, L.; Weissleder, R.; Basilion, J. P. *Bioconj. Chem.* **2000**, *11*, 941.

(9) Shafi, K. V. P. M.; Kolytyn, Y.; Gedanken, A.; Prozorov, R.; Balogh, J.; Lendvai, J.; Felner, I. *J. Phys. Chem. B* **1997**, *101*, 6409.
 (10) Jovalekic, C.; Zdujic, M.; Radakovic, A.; Mitric, M. *Mater. Lett.* **1995**, *24*, 365.
 (11) Manova, E.; Tsoncheva, T.; Paneva, D.; Mitov, I.; Tenchev, K.; Petrov, L. *Appl. Catal., A* **2004**, *277*, 119.
 (12) Yang, H.; Zhang, X.; Tang, A.; Oiu, G. *Chem. Lett.* **2004**, *33*, 826.
 (13) Konishi, Y.; Kawamura, T.; Asai, S. *Ind. Eng. Chem. Res.* **1996**, *35*, 5, 320.
 (14) Sugimoto, T.; Shimotsuna, Y.; Itoh, H. *Powder Technol.* **1998**, *96*, 85.
 (15) Salazar-Alvarez, G.; Muhammed, M.; Zagorodni, A. A. Submitted to *Chem. Mater.*
 (16) Mouden, N.; Pileni, M. P. *Chem. Mater.* **1996**, *8*, 1128.
 (17) Carrazana-Garcia, J. A.; Lopez-Quintela, M. A.; Rivas-Rey, J. *Colloids Surf. A* **1997**, *121*, 61.
 (18) Hoh, J. C.; Yaacob, I. I. *J. Mater. Res.* **2002**, *17*, 3105.
 (19) Tamura, H.; Matijevic, E. *J. Colloid Interface Sci.* **1982**, *90*, 100.
 (20) Pannaparayil, T.; Komarneni, S. *IEEE Trans. Magn.* **1989**, *25*, 4233.
 (21) Kiyama, M. *Bull. Chem. Soc. Jpn.* **1978**, *51*, 134.
 (22) Sugimoto, T.; Matijevic, E. *J. Colloid Interface Sci.* **1980**, *74*, 227.

large batches of materials with reasonable control of composition and particle size.²³ However, the method has received only little attention lately due to the lack of a detailed understanding of the process, leading to the precipitation of nanoparticles with a relatively broad size distribution. The preparation of nanoparticles by using microemulsion methods yields particles with well-defined size and narrow size distribution, but these methods are not suitable to produce large quantities. The coprecipitation method is more advantageous for the production of larger quantities of nanoparticles due to the expense of chemicals and large solvent volumes needed for the microemulsion synthesis. However, the synthesis conditions required for controlling size, shape, and composition of the nanoparticles for larger batches (> 15 g) obtained by the coprecipitation synthesis have not been addressed in the literature.^{24–28}

This paper, which follows a previous paper²⁹ in a series on ferrite nanoparticles and their inclusion in polymer matrixes, addresses the wet synthesis of tens of grams of cobalt ferrite in a stirred reactor with accurate control of chemical composition and average particle size (by nitrogen adsorption measurements) from 50 to 80 nm. The influence of a number of synthesis parameters, including the relative concentrations of metal ions and hydroxide ions in the solutions prior to mixing, the concentration ratio of metal ions to hydroxide ions in the mixed suspension, and digestion time, on the composition, density, crystal structure, morphology, and size distribution of the cobalt ferrite nanoparticles have been studied. The changes in particle size and morphology during digestion have been studied by nitrogen adsorption measurements and transmission electron microscopy.

2. Experimental Section

2.1. Materials. Cobalt chloride hexahydrate ($\text{CoCl}_2 \cdot 6\text{H}_2\text{O}$), ferrous sulfate heptahydrate ($\text{FeSO}_4 \cdot 7\text{H}_2\text{O}$), sodium hydroxide (NaOH), and potassium nitrate (KNO_3) were used for the synthesis of nanoparticle cobalt ferrite (CoFe_2O_4). The chemicals were all of analytical reagent grade or equivalent and they were used as received without further purification. High-purity water (Millipore MILLI-RO 4) with a resistivity of $>10 \text{ M}\Omega\text{-cm}$ was used in all experiments. The walls of all reaction vessels were made hydrophobic by treatment with a 2 vol % solution of methyl-trimethoxysilane as a silylating agent in distilled water for 5 min, rinsed briefly, and cured at 120°C for 60 min.

2.2. Synthesis. Cobalt ferrite nanoparticles were prepared according to the “chemie-douce” method described by Sugimoto and Matijevec.²² An aqueous solution containing cobalt(II) chloride and iron(II) sulfate was heated to 90°C and then transferred to a 2 dm^3 three-neck round-bottom flask containing an aqueous solution of sodium hydroxide and potassium nitrate stirred at 240 rpm also

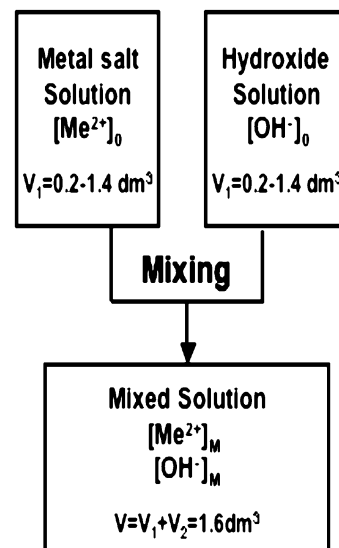


Figure 1. Schematic description of the synthesis procedure. The concentrations of metal ions and hydroxide ions in the two solutions are denoted $[\text{Me}^{2+}]_0$ and $[\text{OH}^-]_0$, respectively. The concentrations of metal ions and hydroxide ions in the mixed solution are denoted $[\text{Me}^{2+}]_M$ and $[\text{OH}^-]_M$, respectively. It should be noted that the volumes of the metal ion solution and the hydroxide solution were varied between 0.2 and 1.4 dm^3 . The volume of the mixed solution was always 1.6 dm^3 .

heated to 90°C . The molar ratio of iron toward cobalt was always 2.0. The potassium nitrate was used as a mild oxidation agent in order to oxidize ferrous ions to ferric ions. The molar ratio of nitrate toward iron(II) was kept constant at 0.66 in all experiments. In earlier reported studies^{19,30,31} this ratio was allowed to vary. After the two solutions were mixed, a black precipitate of nanoparticles was formed immediately. Figure 1 shows schematically the procedure and, in addition, the two concentration ratios— $[\text{Me}^{2+}]_0/[\text{OH}^-]_0$ and $[\text{Me}^{2+}]_M/[\text{OH}^-]_M$ —are defined. The reaction mixture was maintained at 90°C for different periods of time (digestion time) after which a clear solution was decanted from the reaction vessel using a 2.3 T permanent magnet to retain the nanoparticles. These were transferred into a large plastic beaker, washed three times with 5 dm^3 of distilled water, dried overnight at 80°C in air, and milled in a mortar. To ensure reproducibility in the particle synthesis, a setup of two parallel reactors, heated in the same oil bath, was used for each synthesis.

In a first set of experiments, the molar concentration ratio of metal to hydroxide ions of the salt solutions ($[\text{Me}^{2+}]_0/[\text{OH}^-]_0$) prior to mixing was varied by dissolving the salts in different volumes of water. The concentration of the metal ions in the solution prior to mixing varied between 0.189 and 1.320 M; the hydroxide ion concentration in its solution varied between 2.640 and 0.377 M. The final volume after mixing the two solutions was, however, always kept constant at 1.6 dm^3 . The total amounts of metal and hydroxide ions present in the mixed solution were always 0.264 and 0.528 mol, respectively.

In a second set of experiments, the molar ratio of metal ions to hydroxide ions in the mixed solution was varied systematically in a series of experiments. Different amounts of metal salts, ranging from 0.105 to 0.317 mol of metal ions, were dissolved in 1.2 dm^3 of water. The amount of sodium hydroxide was kept constant at 0.528 mol, dissolved in 0.4 dm^3 of water. The initial salt solutions varied as expressed in the $[\text{Me}^{2+}]_0/[\text{OH}^-]_0$ ratio between 0.066 and 0.200.

(23) Willard, M. A.; Kurihara, L. K.; Carpenter, E. E.; Calvin, S.; Harris, V. G. *Int. Mater. Rev.* **2004**, *49*, 125.

(24) Her, Y.; Matijevec, E.; Wilcox, W. R. *Powder Technol.* **1990**, *61*, 173.

(25) Ogihara, T. *J. Soc. Powder Technol. Jpn.* **1994**, *31*, 620.

(26) Matijevec, E. *J. Eur. Ceram. Soc.* **1998**, *18*, 1357.

(27) Ogihara, T. *Fine particles: Synthesis, characterization, and mechanisms of growth*; Marcel Dekker: New York, 2000.

(28) Matijevec, E.; Sapijeszko, R. S. *Fine particles: Synthesis, characterization, and mechanisms of growth*; Marcel Dekker: New York, 2000.

(29) Olsson, R. T.; Hedenqvist, M. S.; Gedde, U. W.; Salazar-Alvarez, G.; Muhammed, M.; Savage, S. *Ninth International Conference on Ferrites*; Soohoo, R., Ed.; American Ceramic Society: New York, p 835.

(30) Matijevec, E. *J. Colloid Interface Sci.* **1987**, *117*, 593.

(31) Tang, Z. X.; Sorensen, C. M.; Klabunde, K. J.; Hadjipanayis, G. C. *J. Colloid Interface Sci.* **1991**, *146*, 38.

During the course of the digestion the evolution of size and morphology of the nanoparticles was studied using 2 cm³ aliquots withdrawn from the reaction vessel after different periods of time. The aliquots were quenched by immediate dilution in 5 times the volume of distilled water and neutralized with acetic acid to pH = 7 before further study. The first withdrawal was made immediately after the addition of the metal salt solution. The last withdrawal was made 120 min after the addition of the metal salt solution.

2.3. Particle Characterization. The chemical composition of the precipitated nanoparticles (concentrations of cobalt and iron) was determined by dissolving a few milligrams in concentrated hydrochloric acid. The solutions were diluted and the cobalt and iron contents were determined by atomic absorption spectroscopy (SpectrAA-220, Varian Inc.).

Crystal phase determinations of the powder samples were obtained by X-ray powder diffraction (XRD) on a Guinier-Hägg camera with focusing geometry using Cu K α radiation ($\lambda = 0.154021$ nm) and Si as internal standard. The cell parameters were refined through the program PIRUM.³²

High-resolution transmission electron micrographs were taken using a JEOL 3010 EX 400 kV electron microscope. Samples of nanoparticles were suspended in ethanol using an ultrasonic horn. A small volume of the suspension was deposited onto an ultrathin carbon-coated 400 mesh copper grid (Ted Pella, Inc.) and dried in air at ~ 40 °C.

Particle size measurements were made from electron micrographs obtained using a JEM 2000EX (JEOL) transmission electron microscope operated at an accelerating voltage of 200 kV and with a Tecnai 10 electron microscope operated at 100 kV. Samples of powders were suspended in ethanol using an ultrasonic horn and small volumes of the suspensions were deposited onto carbon-coated 200 mesh copper grids (Agar Scientific) and dried under a gentle stream of nitrogen. The diameters of more than 1200 particles for each specimen were measured manually on digitized micrographs with the image analysis program Image J.³³ The average particle diameter obtained is referred to as D_{TEM} .

Specific surface area (SSA) of the powders was determined by measuring the nitrogen desorption isotherm in a BET instrument Flowsorb II 2300 (Micromeritics) in single-point area mode. The instrument was calibrated using a Kaolinite standard from Micromeritics. The accuracy of the measurements was tested and the surface area was measured with a precision of 0.2 m²/g. A deviation of 0.2 m²/g is equivalent to a maximum size variation of approximately 1.3 nm. Particle sizes (D_{BET}) were calculated from the specific surface area and the density of the particles assuming spherical or cubic particles.

The density of the particles was determined with an AccuPyc 1330 pycnometer (Micromeritics). The densities were obtained by measuring the displaced volume of helium in a standard 10 cm³ cell with and without particles.

3. Results and Discussion

3.1. Crystal Structure. The X-ray diffraction patterns of the nanoparticles isolated by magnetic decantation after 3 h of digestion, prepared from solutions with different metal ion contents in the mixed solution, are shown in Figure 2. These samples have varying cobalt contents, densities, and different particle shapes, as discussed in sections 3.6 and 3.7. The diffraction patterns are consistent with those reported for spinel cobalt ferrite.^{34,35} The diffraction patterns in Figure

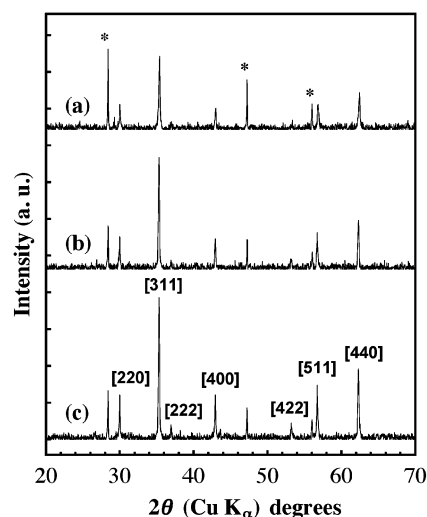


Figure 2. X-ray diffraction patterns from cobalt ferrite nanoparticles for a series of samples digested for 3 h, synthesized from solutions with different $[\text{Me}^{2+}]_{\text{M}}/[\text{OH}^{-}]_{\text{M}}$ ratios: (a) 0.60, (b) 0.50, and (c) 0.40. The marked peaks (*) originated from silicon used as an internal standard.

2 show clear spinel diffraction patterns and do not indicate any presence of an oxyhydroxide phase reported in earlier studies.^{19,21,22} The refined cubic cell axis was determined to 8.394 Å for $[\text{Me}^{2+}]_{\text{M}}/[\text{OH}^{-}]_{\text{M}} = 0.6$; 8.4094 Å for $[\text{Me}^{2+}]_{\text{M}}/[\text{OH}^{-}]_{\text{M}} = 0.5$, and 8.4134 Å for $[\text{Me}^{2+}]_{\text{M}}/[\text{OH}^{-}]_{\text{M}} = 0.4$. Hence, the refined cubic cell axis increases with decreasing $[\text{Me}^{2+}]_{\text{M}}/[\text{OH}^{-}]_{\text{M}}$ ratio. This corresponds to an increase in the lattice parameter with increasing content of cobalt in the structure (see section 3.6). Sorescu et al. used a hydrothermal method to produce cobalt ferrite and reported a linear increase in the lattice parameter with increasing amount of cobalt in the ferrite structure.³⁶

The sharpness of the X-ray diffraction peaks indicates that the material is highly crystalline. This is further supported by the high-resolution electron micrograph displayed in Figure 3. According to Sato et al.,³⁷ the degree of crystallinity of the spinel phase is related to the alkalinity of the precipitation medium. They used a method similar to that for producing MnFe_2O_4 and found that the formation of highly crystalline spinel ferrites was significantly enhanced at $\text{pH} > 11.5$. Synthesis in solutions with lower pH yielded particles with a substantial degree of disorder (amorphous phase). In the present synthesis, the initial pH of the alkaline solution prior to the addition of the metal salt was 12.5. The pH stabilized between 9 and 11 approximately 10 min after the addition of the metal salt solution, with one exception. When the metal ion to hydroxide ion ratio in the mixed suspension was equal to 0.6, the pH stabilized at 6.6.

3.2. Effect of Digestion Time on the Particle Morphology. Figure 4 shows electron micrographs of aliquots taken after digestion times between 0 and 180 min. The lower metal ion concentration with respect to the hydroxide ion concen-

(32) Werner, P.-E. *Ark. Kemi* **1969**, *31*, 513.

(33) <http://rsb.info.nih.gov/ij/> (2003-11-04).

(34) Gallagher, K. J.; Feitknecht, W.; Mannweiler, U. *Nature* **1968**, *217*, 1118.

(35) Cornell, R. M.; Schwertmann, U. *The Iron Oxides*, 2nd ed.; Wiley-VCH: Weinheim, Germany, 2003.

(36) Sorescu, M.; Grabias, A.; Tarabasnu-Mihaila, D.; Diamandescu, L. *J. Mater. Synth. Process.* **2001**, *9*, 119.

(37) Sato, T.; Kuroda, C.; Saito, M. *Ferrites: Proc. Int. Conf. Jpn.* **1970**, *72*.

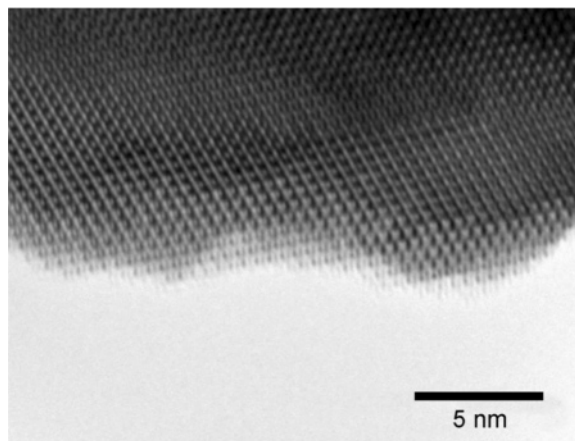


Figure 3. High-resolution transmission electron micrograph of a 50 nm cobalt ferrite nanoparticle. Digestion time: 3 h. Synthesis conditions: $[\text{Me}^{2+}]_0/[\text{OH}^-]_0 = 0.167$; $[\text{Me}^{2+}]_M/[\text{OH}^-]_M = 0.50$.

tration in the mixed suspension, $[\text{Me}^{2+}]_M/[\text{OH}^-]_M = 0.3$, yielded a more slowly changing particle system due to the lower concentration of soluble species in solution, and it was possible to follow the particle growth using the sampling procedure described. Upon heating the metal ion solution to 90 °C prior to the precipitation, the acidic conditions and the relatively slow heating rate induced the formation of an orange-brownish sol composed of an iron oxyhydroxide phase. Initially, the metal ion solution was transparent dark red. Raming et al. observed the formation of a similar sol and reported the formation of an oxyhydroxide phase together with hematite phase when an iron(III) chloride solution is heated slowly in acidic media.³⁸ In this work, the hematite phase was not obtained since it is known to precipitate after longer aging times (>1 day).³⁹ The mixed suspension immediately became dark brown or black on the addition of the metal salt solution to the hydroxide solution. The first aliquot, withdrawn immediately after mixing the two solutions, contained a large number of hexagonal and triangular platelets (Figure 4a). Similar platelets have been observed in samples taken from aqueous coprecipitation systems yielding iron and manganese ferrite particles.^{22,31} The red-brownish color of the sample deposited on the TEM grid and the relatively high reduction potential of the suspension suggest that the platelets consist of δ -FeOOH. No spherical or cubic particles were observed in this sample.

The aliquot withdrawn after 1 min consisted mostly of hexagonal and triangular platelets and a few acicular and spherical particles (Figure 4b). The largest spherical particles in this sample had a diameter of approximately 60 nm. The aliquot withdrawn after 5 min showed many platelets, acicular particles, and spherical particles. The spherical particles had a diameter of 90–100 nm (Figure 4c). The platelets and acicular particles were also observed in the 10 min sample together with a large number of spherical particles; the latter had a maximum diameter of 130–140 nm (Figure 4d). The aliquot withdrawn after 20 min contained no acicular particles and only a few platelets, which at this stage had grown very large, 200–500 nm (Figure 4e).

The largest spherical particles had a diameter of 160 nm and a few of the smaller particles (30–40 nm) showed tendencies to cubical shapes. A large number of very small (5–10 nm) equiaxed particles were also observed in this sample (not depicted). These small particles are assumed to be formed from the unstable platelets. The observation made on the sample withdrawn after 30 min (Figure 4f) is consistent with this assumption: the platelets were completely absent and the fraction of the small equiaxed particles (5–10 nm) had increased significantly with respect to that in the sample withdrawn after 20 min. In addition, larger and clearly cubical particles were observed in this sample. The aliquots withdrawn after digestion times longer than 30 min showed no further change in particle morphology.

The shape of ferrite nanoparticles can be controlled by adjusting the particle growth rate by varying the temperature.⁴⁰ Higher temperatures and concomitantly enhanced growth rates usually favor the formation of spherical particles as a result of less selective crystallographic growth direction. In the present case, the growth rate decayed with time as the concentration of metal ions in solution decreased and the digestion proceeded. Figure 4g displays the sample obtained after 3 h of digestion followed by washing and magnetic decantation. The small particles were not present due to the magnetic decantation and the dominant feature was spherical and rounded cubic single particles without any visible internal structure.

The X-ray diffraction patterns presented in Figure 5 indicate that the initially formed (after 1 min) nanoparticles consist of two separate phases: the spinel phase and δ -FeOOH. The identification of the phases was made according to Cornell and Schwertmann.³⁵ The diffraction peaks associated with the δ -FeOOH phase appearing at $2\theta \approx 41^\circ$ and 53° decreased markedly with increasing digestion time and the sample digested for 30 min shows essentially no peak at $2\theta \approx 41^\circ$ (Figure 5).

Traces of a secondary phase appearing as a small peak at $2\theta \approx 44^\circ$ were reported in a previous paper.²⁹ Nanoparticles synthesized according to the very same procedure as was used in the previous paper, and analyzed using high-resolution X-ray diffraction, show no traces of a second phase. It seems likely that the samples obtained after 3 h digestion consist of a pure spinel phase, and only in a few cases can they contain traces of an impurity appearing as a peak at $2\theta \approx 44^\circ$. The magnetic character of the platelets and the electron diffraction pattern of the same structure suggest that δ -FeOOH was present at the initial stages of particle growth and we propose that this phase was in the later stages converted into $\text{Co}_x\text{Fe}_{3-x}\text{O}_4$. The oxyhydroxide phase has a low energy for nucleation³⁵ and it forms first; however, the spinel phase has a lower solubility constant,^{35,41} which results in the formation of spinel with long aging times. Hence, the early-proposed mechanism of dissolution/re-crystallization may apply.^{42,43} This conversion of the oxyhydroxide phase into the spinel phase may also be

(38) Raming, T. P.; Winnbust, A. J. A.; van Kats, C. M.; Philipse, A. P. *J. Colloid Interface Sci.* **2002**, *249*, 346.

(39) Matijevic, E.; Schneider, P. *J. Colloid Interface Sci.* **1978**, *63*, 509.

(40) Song, Q.; Zhang, Z. *J. Am. Chem. Soc.* **2004**, *126*, 6164.

(41) Kelén, T.; Wijkström, H.; Ahlberg, E. *The Swedish Radiation Protection Authority, SSI. Project report SSI-P-1331*, 2003.

(42) Schwertmann, U.; Murad, E. *Clays Clay Miner.* **1983**, *31*, 277.

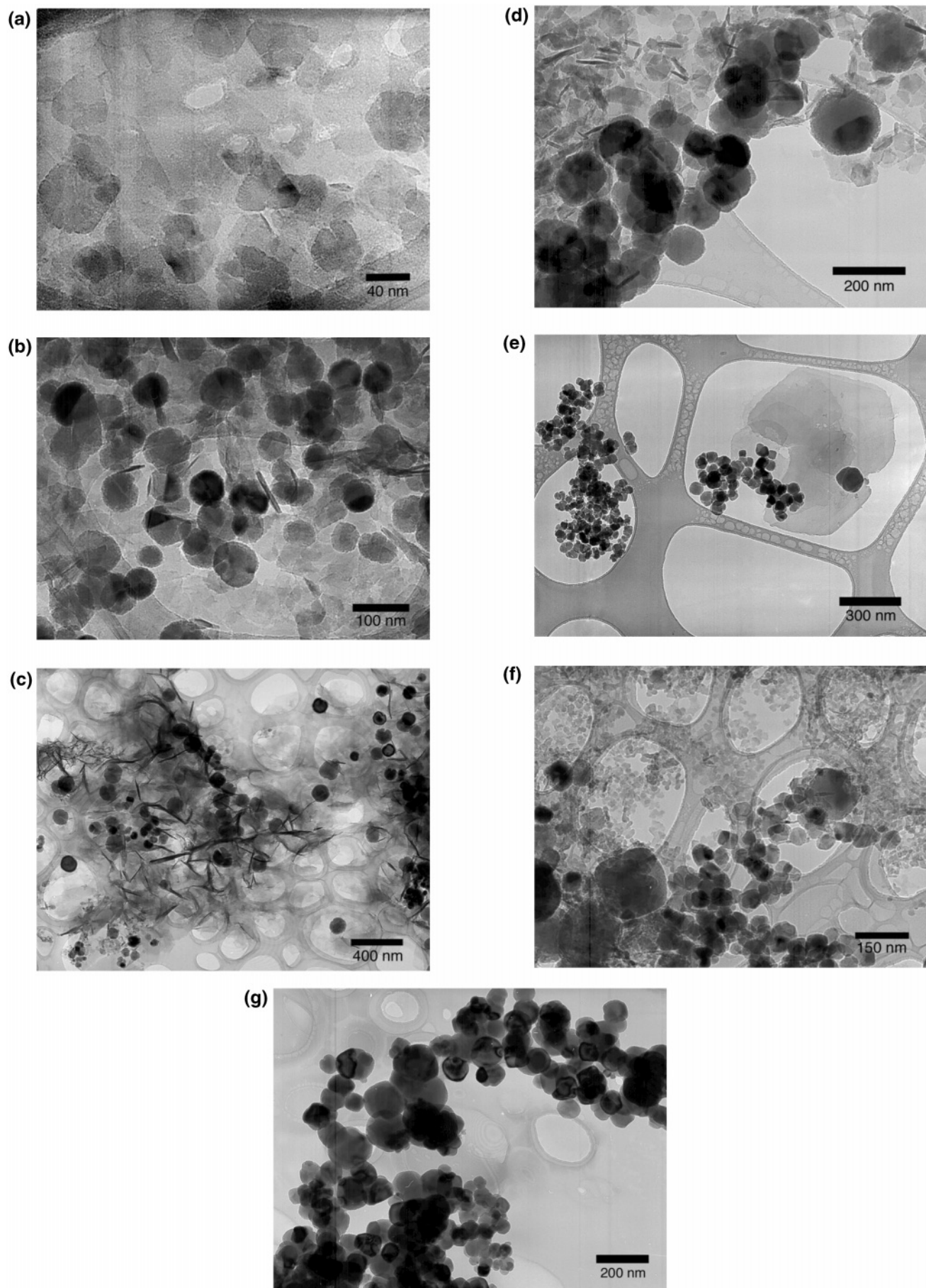


Figure 4. Transmission electron micrographs of cobalt ferrite nanoparticles (synthesis conditions: $[\text{Me}^{2+}]_0/[\text{OH}^-]_0 = 0.100$; $[\text{Me}^{2+}]_M/[\text{OH}^-]_M = 0.30$) after different periods of digestion: (a) 0 min; (b) 1 min; (c) 5 min; (d) 10 min; (e) 20 min; (f) 30 min; (g) 180 min.

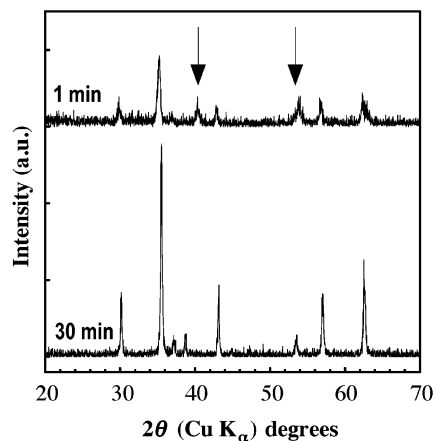


Figure 5. X-ray diffraction patterns of cobalt ferrite nanoparticles obtained after different periods of digestion: (a) 1 min; (b) 30 min. Conditions of the synthesis: $[\text{Me}^{2+}]_0/[\text{OH}^-]_0 = 0.133$; $[\text{Me}^{2+}]_M/[\text{OH}^-]_M = 0.40$. The arrows indicate peaks associated with the δ -FeOOH phase.

responsible for the broad particle size distributions that are obtained.

3.3. Assessment of Average Particle Size. The results of particle size determinations by nitrogen adsorption measurement (BET) and transmission electron microscopy from a series of samples are compared in Figure 6. The number average particle size as determined by transmission electron microscopy ($\langle D_{\text{TEM}} \rangle$) was 10–20 nm smaller than the corresponding average size obtained by nitrogen adsorption. The average particle size obtained by nitrogen adsorption is derived from the surface area of a given sample mass. The total surface area (A) of a group of spherical particles with diameters D_i is

$$A = \pi \sum_i D_i^2 \quad (1)$$

The mass (m) of the corresponding group of spherical particles is

$$m = \frac{\rho\pi}{6} \sum_i D_i^3 \quad (2)$$

where ρ is the density. The specific surface area (SSA) is thus given by

$$\text{SSA} = \frac{A}{m} = \frac{6}{\rho \times \sum_i D_i^3 / \sum_i D_i^2} \quad (3)$$

The average particle diameter (D_{BET}) is thus given by

$$D_{\text{BET}} = \frac{\sum_i D_i^3}{\sum_i D_i^2} = \frac{6}{\rho \times \text{SSA}} \quad (4)$$

Equation 4 also is valid for a group of cubic particles with edge lengths D_i . It should be noted that D_{BET} is not a number average of the particle diameters.

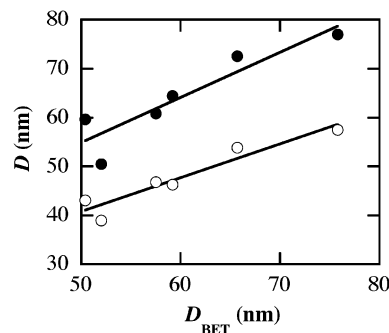


Figure 6. Comparison between nanoparticle size average determinations by transmission electron microscopy and nitrogen adsorption measurements (D_{BET}). $\langle D_{\text{TEM}} \rangle$: \circ (number average) and D'_{BET} : \bullet (eq 5). Line is added as an aid to the eye only.

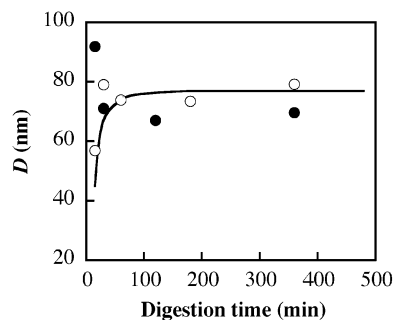


Figure 7. Average particle size according to nitrogen adsorption measurements (D_{BET} : \circ) and transmission electron microscopy (D'_{BET} : \bullet (eq 5)) as a function of the digestion time. Synthesis conditions: $[\text{Me}^{2+}]_0/[\text{OH}^-]_0 = 0.133$; $[\text{Me}^{2+}]_M/[\text{OH}^-]_M = 0.40$.

From the manual measuring of particles depicted by transmission electron microscopy (D_{TEM}), an apparent particle size was calculated and is given by

$$D'_{\text{BET}} = \langle D_{\text{TEM}}^3 \rangle / \langle D_{\text{TEM}}^2 \rangle \quad (5)$$

This apparent particle size was compared with D_{BET} obtained by nitrogen adsorption measurements (Figure 6). The deviation between the two averages is only ~ 3 nm; the diameter based on transmission electron microscopy images being higher ($D_{\text{BET}} \sim D'_{\text{BET}}$). This relatively small difference in average size estimate may be related to differences in the sampling procedure; the smaller particles were more efficiently sampled for the nitrogen adsorption measurements.

The two methods have advantages and disadvantages for particle size determination. Nitrogen adsorption measurements provide results with a high degree of repeatability. The time required for each analysis was short, on average 10 min. Transmission electron microscopy also yielded averages with a high degree of repeatability provided that a sufficiently large number (~ 1000) particles were included in the statistics. Furthermore, transmission electron microscopy provided information about the particle size distribution and the particle shape. The time required for each analysis was however very long, ~ 1000 min.

3.4. Effect of the Digestion Time on Average Particle Size and Size Distribution. Figure 7 shows the effect of digestion time on the average particle size as determined by nitrogen adsorption and transmission electron microscopy. It should be noted that the analyses are based on samples obtained by magnetic decantation and washing. The 15 min

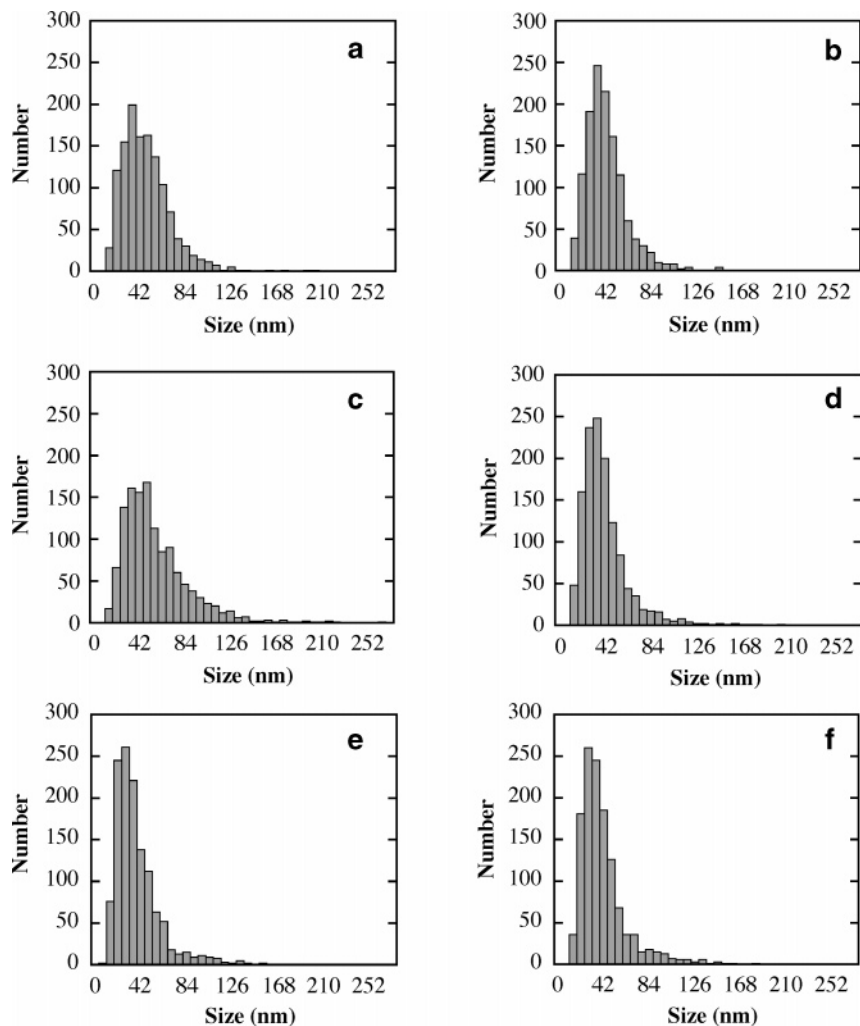


Figure 8. Particle size distributions obtained by transmission electron microscopy of a series of samples synthesized with different digestion times: (a) 1 min; (b) 8 min; (c) 15 min; (d) 30 min; (e) 120 min; (f) 180 min. Synthesis conditions: $[\text{Me}^{2+}]_0/[\text{OH}^-]_0 = 0.133$; $[\text{Me}^{2+}]_M/[\text{OH}^-]_M = 0.40$.

batch contained particles with an average size of 56 nm (D_{BET}). After 30 min of digestion or longer, the average particle size stabilized between 70 and 80 nm (D_{BET}). The D_{BET} values (eq 5) were close to the range of the D_{BET} values obtained by the nitrogen adsorption measurements for the samples digested longer than 30 min. However, the samples digested for 15 min or less showed a large deviation between the two particle sizes. This is explained by the fact that the nanoparticles were mainly platelets and in some cases acicular particles. Equation 5 does not apply for these geometries.

Figure 8 shows the size distributions of magnetically decanted batches digested for different times. Particle sizes ranged from 20 to 160 nm with a majority between 40 and 50 nm. The size distribution varied for batches digested at shorter times (<30 min), which is attributed to the morphological transformation from platelets to equiaxed particles. After 30 min and on prolonged digestion, the size distribution remained essentially the same in accordance with the average particle size data obtained by nitrogen adsorption measurements (Figure 7). The narrowing of the size distributions with increasing digestion time was slightly more pronounced in the case of aliquots²⁹ (when particles were not isolated by magnetic forces).

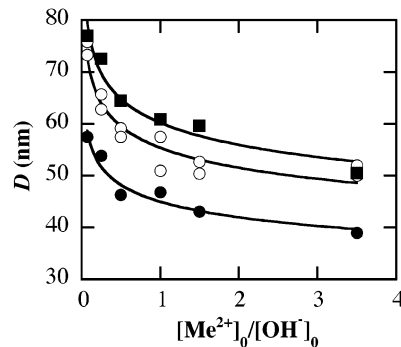


Figure 9. Average particle size according to nitrogen adsorption measurements (D_{BET} : \circ) and transmission electron microscopy ($\langle D_{\text{TEM}} \rangle$: \bullet (number average) and D_{BET} : \blacksquare (eq 5)) as a function of the metal ion to hydroxide ion concentration ratio of the solutions before mixing, $[\text{Me}^{2+}]_0/[\text{OH}^-]_0$. The data from nitrogen adsorption measurement are from Olsson et al.²⁷ The continuous lines are third polynomial fits to the experimental data.

3.5. Effect of Concentration of Metal Ions to Hydroxide Ions in the Solutions Prior to Mixing on the Average Size of the Particles. Figure 9 shows the effect of concentration ratio of Me^{2+} and OH^- in the solutions prior to mixing ($[\text{Me}^{2+}]_0/[\text{OH}^-]_0$) on the average particle size by nitrogen adsorption measurements and transmission electron microscopy. The particle size data obtained by nitrogen adsorption

have been reported earlier²⁹ and they serve as a comparison to the new data obtained by transmission electron microscopy. It was concluded in the previous paper²⁹ that varying $[\text{Me}^{2+}]_0/[\text{OH}^-]_0$ and keeping the mixed suspension volume constant made it possible to reproduce particles within a 5 nm range with average sizes between 50 and 80 nm. The assessments of the average particle size by transmission electron microscopy, using the same type of average as obtained from the nitrogen adsorption measurements (eq 5), yield a similar trend in the data for particle size and $[\text{Me}^{2+}]_0/[\text{OH}^-]_0$. The size values, however, are ~ 3 nm larger than for the corresponding data obtained by the nitrogen adsorption measurements (see discussion in section 3.3). The new data obtained by transmission electron microscopy confirm the previously stated conclusion (based on nitrogen adsorption measurements) that average particle size can be controlled within a 5 nm range by adjusting $[\text{Me}^{2+}]_0/[\text{OH}^-]_0$. The number average particle size values range according to transmission electron microscopy between 35 and 60 nm. The density of the nanoparticles increased only moderately with increasing $[\text{Me}^{2+}]_0/[\text{OH}^-]_0$.

The results show that particles become smaller when more concentrated metal salt solutions are used. This suggests that the conditions prevailing during the first seconds after the mixing of the two solutions determine the outcome. It may be argued, in agreement with Söhnel and Garside,⁴⁴ that the nucleation rate increases with increasing metal ion content in the metal salt solution. Thus, the number of particle nuclei formed would be higher from the more concentrated metal ion solution, which would obviously lead to the formation of a greater number of smaller particles. Chinnasamy et al. used a different approach to decrease the size of the cobalt ferrite nanoparticles by coprecipitating various fractions of ferric/ferrous ions together with cobalt ions (Co:Fe; 1:2). They obtained smaller particles with an increasing fraction of ferric ions and the average grain size ranged between 15 and 55 nm, as determined by XRD.⁴⁵

The morphology (fraction cubic vs spherical) of the particles after 3 h of digestion did not seem to be dependent on the $[\text{Me}^{2+}]_0/[\text{OH}^-]_0$. All systems with $[\text{Me}^{2+}]_M/[\text{OH}^-]_M = 0.5$ generated the same fraction of sharp-edged cubical particles (see section 3.7).

3.6. Effect of Metal Ion to Hydroxide Ion Concentration Ratio in the Mixed Suspension on Mature Particle Composition and Density. Figure 10 shows that the cobalt content in the particles can be varied in a controlled manner by varying the metal ion to hydroxide ion concentration ratio in the mixed solution, $[\text{Me}^{2+}]_M/[\text{OH}^-]_M$. Some of the data points showed significant deviation, but the overall trend is clear.

Note that this shows that the composition of the precipitated nanoparticles varied, although the initial iron to cobalt ratio prior to mixing was constant and consistent with the stoichiometric composition. It has been reported that control of the particle composition can also be achieved by varying

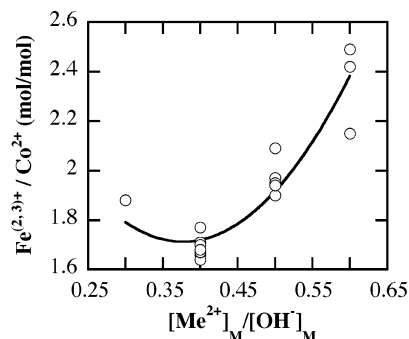


Figure 10. Iron/cobalt molar ratio of nanoparticles as a function of the metal ion–hydroxide ion molar ratio of the mixed suspension, $[\text{Me}^{2+}]_M/[\text{OH}^-]_M$. The digestion time was 3 h. Line is only to show the trend.

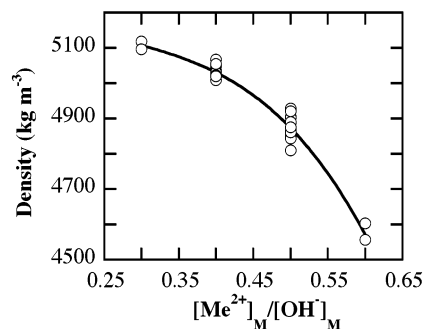


Figure 11. Density of nanoparticles as a function of the metal ion–hydroxide ion molar ratio of the mixed suspension, $[\text{Me}^{2+}]_M/[\text{OH}^-]_M$. The digestion time was 3 h. Line is only to show the trend.

the initial iron to cobalt ratio.^{19,46,47} Similar results on the variation of composition have been reported by Kiyama,²¹ who employed a slightly different chemical synthesis for the preparation of cobalt ferrite using higher metal to hydroxide ratios and a slightly lower temperature (~ 70 °C). He reported that the cobalt content expressed in x ($\text{Co}_x\text{Fe}_{3-x}\text{O}_4$) could be adjusted between 0.05 and 3. In the present study, nanoparticles with a cobalt composition corresponding to x values in the range 0.86–1.14 were synthesized. The changes in composition obtained by varying $[\text{Me}^{2+}]_M/[\text{OH}^-]_M$ may originate from the different rates of formation of the metal hydroxides. The oxidation of Fe(II) is catalyzed by an excess of hydroxide, which is a condition prevailing at low values of $[\text{Me}^{2+}]_M/[\text{OH}^-]_M$. The fast transformation of Fe(II) to Fe(III) at high pH facilitates the formation of the spinel phase.³⁵ At a low concentration of hydroxide ions (high values of $[\text{Me}^{2+}]_M/[\text{OH}^-]_M$), larger amounts of Fe(II) species are formed in the solution, which at a later stage transform into $\text{Fe}(\text{OH})_3$ and $\delta\text{-FeOOH}$.

Figure 11 shows the variation in density with increasing $[\text{Me}^{2+}]_M/[\text{OH}^-]_M$. The change in density, which can be attributed to increasing cobalt content in the spinel phase, is at most 2%, which is considerably less than the observed decrease in density (8%) displayed in Figure 12. The unit cell parameter data presented in section 3.1 indicate an increase in density by approximately 0.5% with increasing cobalt content. One tentative explanation to the pronounced decrease in density would be to assign it to a gradual increase in the proportion of amorphous $\text{Fe}(\text{OH})_3$ and $\delta\text{-FeOOH}$

(44) Söhnel, O.; Garside, J. *Precipitation: Basic principles and industrial applications*; Butterworth-Heinemann: Oxford, UK, 1992.

(45) Chinnasamy, C. N.; Senoue, M.; Jeyadevan, B.; Peralez-Perez, O.; Shinoda, K.; Tohji, K. *J. Colloid Interface Sci.* **2003**, *263*, 80.

(46) Tourinho, F. A.; Franck, R.; Massart, R. *J. Mater. Sci.* **1990**, *25*, 3249.

(47) Li, X.; Kutal, C. *J. Alloys Compd.* **2003**, *349*, 264.

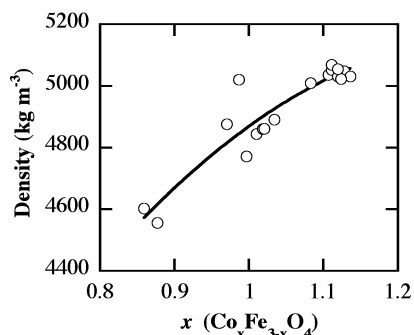


Figure 12. Density of nanoparticles as a function of cobalt content (expressed as x ; $\text{Co}_x\text{Fe}_{3-x}\text{O}_4$). The data were obtained from the data shown in Figures 10 and 11.

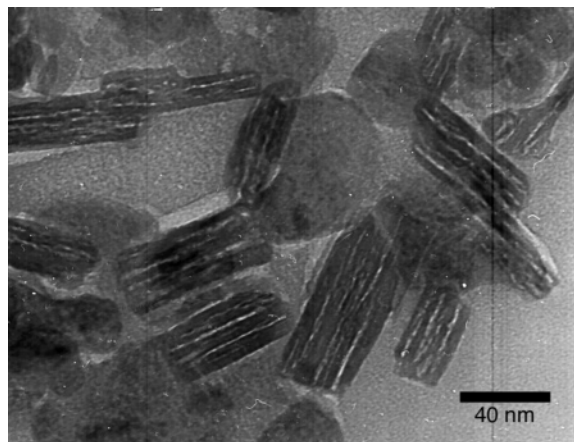


Figure 13. Transmission electron micrograph showing the porous structures in particles synthesized at $[\text{Me}^{2+}]_0/[\text{OH}^-]_0 = 0.066$ and $[\text{Me}^{2+}]_M/[\text{OH}^-]_M = 0.2$.

species in the nanoparticles. The densities of $\text{Fe}(\text{OH})_3$ and $\delta\text{-FeOOH}$ have been reported to 3120 and 4260 kg m^{-3} , respectively,⁴⁸ which are considerable lower than that of the cobalt ferrite spinel phase, which is in excess of 5300 kg m^{-3} .⁴ Also, the variation in densities could originate from entrapped nanoporous structures, which are formed during the transformation of $\delta\text{-FeOOH}$ to the spinel phase. The formation of such structures was earlier reported for the transformation of $\alpha\text{-FeOOH}$ into $\alpha\text{-Fe}_2\text{O}_3$.^{49,50} Similar channels were observed in particles prepared with $[\text{Me}^{2+}]_0/[\text{OH}^-]_0 = 0.066$ and $[\text{Me}^{2+}]_M/[\text{OH}^-]_M = 0.2$ and are shown in Figure 13. The particles were rodlike with a length of 40–80 nm and a thickness of 20–30 nm. The pores with a diameter of approximately 1–3 nm appeared parallel to the length of the particles. The yield of the reaction under these conditions was very low, even after long digestion. The porous structures were a very small fraction of the magnetically decanted particles. Hence, there are no solid reasons to believe that porous structures account for the large variations in density.

3.7. Effect of Metal to Hydroxide Ratio on the Mature Particle Morphology. After 3 h of digestion, the final particles showed various morphologies depending on the

(48) Lide, D., Ed. *CRC Handbook of Chemistry and Physics, 85 Ed.*; CRC Press: Boca Raton, FL, 2004.

(49) Pomiès, M. P.; Morin, G.; Vignaud, C. *Eur. J. Solid State Inorg. Chem.* **1998**, *35*, 9.

(50) Watari, F.; Delavignette, P.; Van Landuyt, J.; Amelinckx, S. *J. Solid State Chem.* **1983**, *48*, 49.

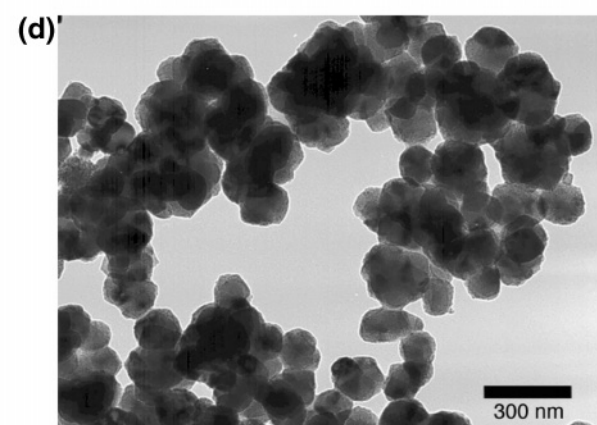
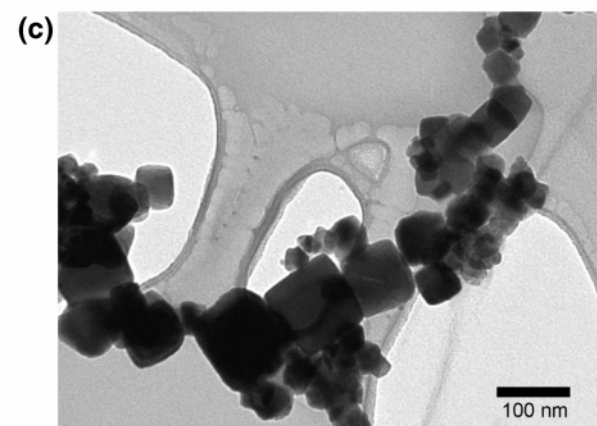
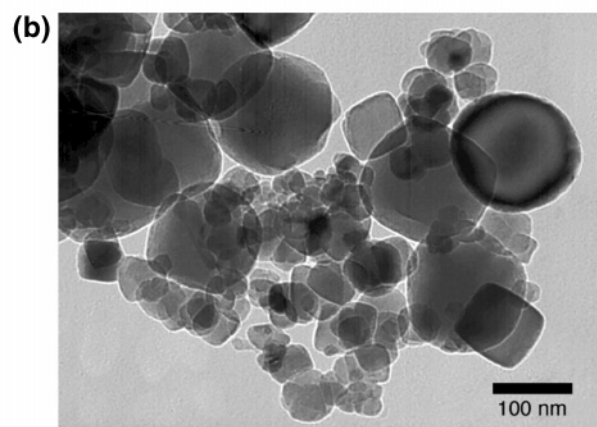
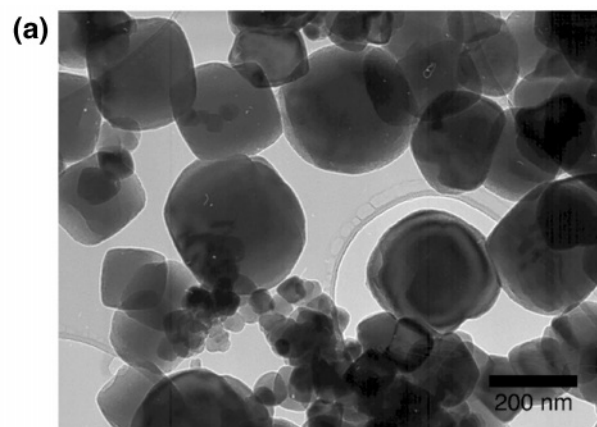


Figure 14. Transmission electron micrographs of nanoparticles synthesized for 3 h from suspensions with the following $[\text{Me}^{2+}]_M/[\text{OH}^-]_M$ ratios: (a) 0.30; (b) 0.40; (c) 0.50 (d) 0.60. Digestion time, 3 h, followed by magnetic decantation.

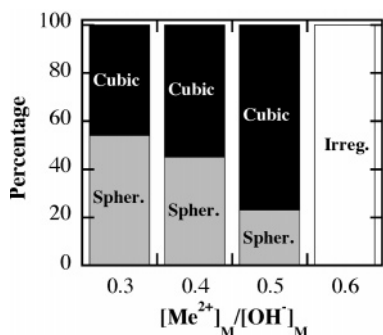


Figure 15. Histograms showing the frequency of different particle shapes (cubic, spherical, and irregular) for particles isolated by magnetic decantation after 3 h of digestion. The different bars refer to mixed solutions with different $[\text{Me}^{2+}]_{\text{M}}/[\text{OH}^{-}]_{\text{M}}$ ratios as shown below the x -axis.

metal ion/hydroxide ion concentration ratios used for the precipitation (Figure 14).

The solution with the lowest metal ion content, $[\text{Me}^{2+}]_{\text{M}}/[\text{OH}^{-}]_{\text{M}} = 0.3$, yielded cobalt-rich particles with a high density, 5120 kg m^{-3} . These particles were mostly spherical/rounded cubic (Figure 14a). As the amount of metal ions used for the precipitation was increased, the fraction of cubic particles increased (Figure 14b). For the composition close to the stoichiometric value for cobalt ferrite (CoFe_2O_4), clearly cubic particles with sharp edges were in large excess (Figure 14c). A further increase in the amount of metal ions, $[\text{Me}^{2+}]_{\text{M}}/[\text{OH}^{-}]_{\text{M}} = 0.6$, yielded mostly irregular particles with rough surfaces. Spherical nanoparticles were also present but only as a small fraction (Figure 14d).

TEM micrographs were analyzed manually, and the statistical distribution of cubic and spherical nanoparticles was evaluated. Figure 15 presents a summary of the proportions of the different particle shapes as a function of metal ion concentration. For a given metal ion concentration, the statistical distribution of cubic and spherical particles did not vary with the initial concentration ratio $[\text{Me}^{2+}]_0/[\text{OH}^{-}]_0$ at a given $[\text{Me}^{2+}]_{\text{M}}/[\text{OH}^{-}]_{\text{M}}$.

The shape of ferrite nanoparticles can be controlled by adjusting the particle growth rate by varying the temperature.⁴⁰ Higher temperatures and faster growth rate usually favor the formation of spherical particles as a result of less selective crystallographic growth direction. In the present study, the morphology was related to the amount of metal ions used for the precipitation of particles in the alkaline solution and to the concentration of metal ions in the mixed system since the temperature was kept constant. The explanation to the varying fraction of cubic to spherical particles in the final powders is most likely a result of the variation in growth rate between the different systems. Low values of $[\text{Me}^{2+}]_{\text{M}}/[\text{OH}^{-}]_{\text{M}}$ generated predominately spherical particles and rounded cubes. This system was also the first system to generate a clear solution; thus, the conversion of $\delta\text{-FeOOH}$ into spinel phase was the fastest. As the $[\text{Me}^{2+}]_{\text{M}}/[\text{OH}^{-}]_{\text{M}}$ ratio was increased and the alkalinity decreased, the transformation between the two phases proceeded for longer

times and after certain digestion times the dissolution of $\delta\text{-FeOOH}$ and nucleation of spinel phase had slowed to an extent where the growth rate favored the formation of cubic particles. The fraction of spherical and rounded cubical particles in this system may originate from the spinel particles that precipitated first. Hence, low $[\text{Me}^{2+}]_{\text{M}}/[\text{OH}^{-}]_{\text{M}}$ (high alkalinity) favored the formation of spinel phase whereas a high ratio (low alkalinity) delayed the formation of spinel, which resulted in cubic particles.

4. Conclusions

Among several methods to produce ferrite nanoparticles in larger quantities, precipitation of metallic ions from an alkaline aqueous medium is an efficient, economic and environmentally benign method to obtain larger quantities of particles for applied research. It is possible to control the size, size distribution, composition, and density of the particles within relatively narrow margins by adjusting the molar ratio of metal ion to hydroxide ion in the reaction vessel. For a constant metal ion to hydroxide ion molar ratio in the mixed solution, it was possible to control the average size of the particles to within 5 nm by varying the initial ion concentrations of the precipitants before mixing. The average sizes of the nanoparticles were between 50 and 80 nm according to nitrogen adsorption measurements, which for the present particle size distributions is in accordance with the number average range 35–60 nm. The density and composition of the particles were closely related and nanoparticles with super-stoichiometric content of cobalt had the highest densities. The variation in densities could not be explained solely from the variation in metal ions composition in the particles. The presence of different phases such as oxyhydroxides and even different morphologies (nanoporous structures) could also result in large variations of the macroscopic density of the materials. Particle size distributions revealed that digestion led to a narrowing of the particle size distribution, favoring formation of particles in the 40–50 nm size range, whereas larger particles (70–190 nm) became less frequent with increasing digestion time. The variation in particle size distribution is explained by a gradual morphology/phase transformation from initial precipitated $\delta\text{-FeOOH}$ platelets to cubic or spherically shaped spinel phase nanoparticles. Finally, the morphology of the nanoparticles changed with increasing concentration of the metal ion solution from mostly spherical to mostly sharp edge cubical with smooth surfaces, and further to spherical/irregular with a rough surface texture.

Acknowledgment. The financial support from the Swedish Defense Research Agency (FOI), Linköping, Sweden, is gratefully acknowledged. The scholarship for G.S.A. provided by KTH Rektors gåvomedel is acknowledged. The authors thank Prof. Mamoun Muhammed for valuable comments.

CM0501665